Proceedings of the Combustion Institute 42 (2026) 106144

Contents lists available at ScienceDirect

Proceedings of the Combustion Institute

journal homepage: www.elsevier.com/locate/proci

Scaling law for the oblique-detonation-wave/boundary-layer interaction length

Xiaotong Tong [a], Yufeng Wang [b], Zheng Chen [a,*]

[a] SKLTCS, HEDPS, School of Mechanics and Engineering Science, Peking University, Beijing, 100871, China
[b] College of Engineering Science, Peking University, Beijing, 100871, China

ARTICLE INFO

Keywords:
Oblique detonation wave
Boundary layer
Flow separation
Scaling law

ABSTRACT

The oblique-detonation-wave/boundary-layer interaction (ODWBLI) significantly affects the performance and robustness of an oblique-detonation engine. However, studies on the scale of ODWBLI and its underlying scaling law remain limited. This work investigates the separation flow regime under different static pressures and wall temperatures through two-dimensional simulations considering detailed chemistry. It is found that the heat release rate within the reacting boundary layer partially counteracts the effect of wall cooling, rendering the dimensionless interaction length in reacting flow less sensitive to the skin-friction coefficient than in non-reacting flow. In reacting flow, the increase of separation scale relative to non-reacting flow is attributed to the balance between the dissipation of the gas kinetic energy and combustion heat release. To quantitatively estimate the separation scale, the heat release behind the separation shock wave and the separation oblique detonation wave is analyzed. Based on the energy-conservation relation within the separation bubble, an effective heat release rate is proposed and expressed as a function of Reynolds number and reference temperature. By incorporating a correction factor to account for the expansion wave emanating from the wedge trailing edge, a generalized scaling law for both non-reacting and reacting ODWBLI length is established. This scaling law offers useful guidance for the design of oblique detonation engines.

Novelty and significance statement

Unlike the existing studies on the inviscid reflection of oblique detonation waves (ODWs), this work numerically and theoretically investigates the viscous boundary-layer separation regime induced by ODWs. Moreover, the existing non-reacting theories for shock-wave/boundary-layer interaction are not applicable to reacting flows. In this paper, the coupling mechanism between viscous flow and chemical reaction is elucidated. For the first time, a scaling law for the length of oblique-detonation-wave/boundary-layer interaction length is proposed.

Boundary-layer separation induced by detonation or shock waves poses a risk to practical air-breathing combustors. Currently, estimating the interaction scale in reacting flow remains challenging, leading to combustor designs that demand extensive computational and experimental resources. The scaling law proposed in this study provides a valuable tool for the design of oblique detonation engines.

1. Introduction

The oblique detonation engine (ODE) is a promising propulsion technology for hypersonic flight above Mach 10 [1]. In an ODE combustor, the boundary-layer separation [2] induced by an incident oblique detonation wave (ODW) may lead to excessive wall friction and thermal loads [3]. It can even destabilize the incident ODW by choking the combustor throat [4–5]. Therefore, the viscous effects and boundary-layer separation are crucial for the design of ODE.

Unfortunately, most existing studies have focused either on the reflection of ODWs in ideal inviscid flow or on the qualitative evolution of separation regions. For example, Yan et al. [6] investigated the topology of a curved detonation wave and its reflection in a contraction duct; Zhang et al. [7] examined the stabilization characteristics and mechanisms of ODWs in a typical ODE combustor; Sun et al. [8] explored the destabilization patterns of ODW-induced boundary-layer separation in hypersonic reactive flow. However, quantitative laws describing the stable separation scale—essential for combustor design—have not been established in previous work.

Since the separation scale in non-reacting flow has been well studied

* Corresponding author.
E-mail address: cz@pku.edu.cn (Z. Chen).

https://doi.org/10.1016/j.proci.2026.106144
Received 15 March 2026; Accepted 6 June 2026
Available online 8 July 2026

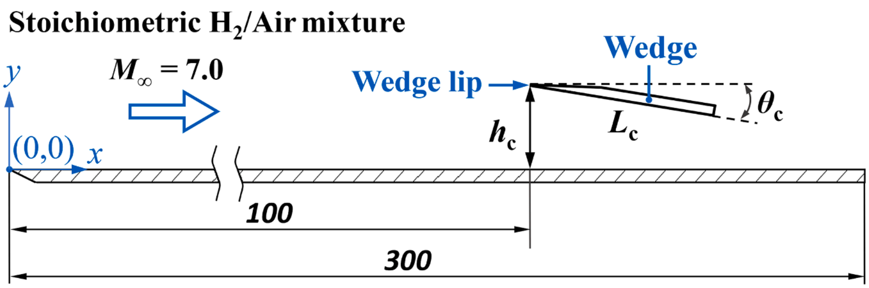

Fig. 1. Schematic of computational domain.

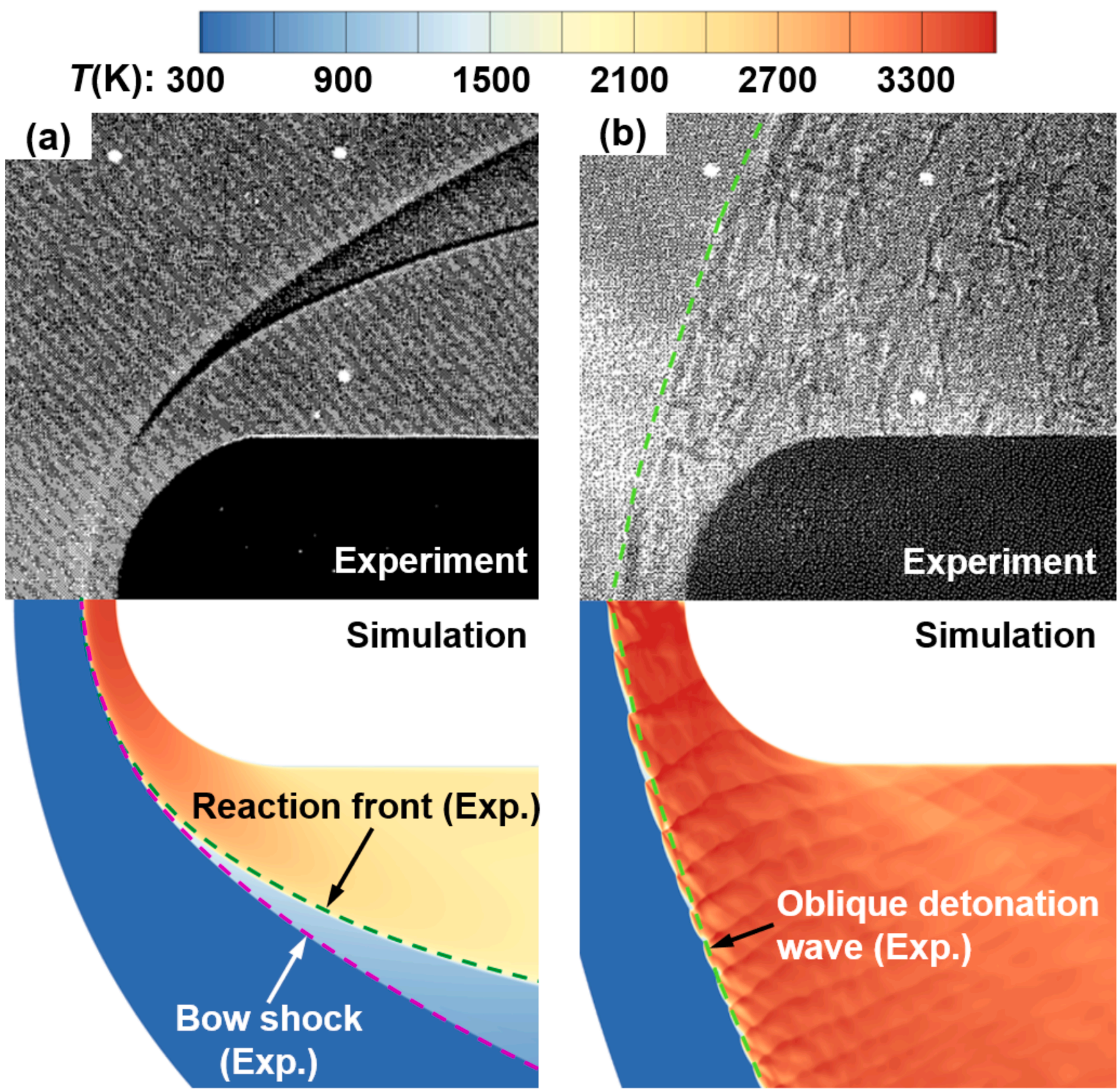

Fig. 2. Reacting flow validation: (a) shock-induced combustion in hydrogen/air; (b) overdriven ODW in hydrogen/oxygen.

in the literature [9], this paper aims to develop an estimation method by extending existing scaling laws for non-reacting flow. Souverein et al. [9] proposed the following similarity parameter for the length of shock-wave/boundary-layer interaction:

$$L^* = \frac{L_{\rm int}}{\delta^*}\frac{\sin\beta_{\rm c}\sin\theta_{\rm c}}{\sin(\beta_{\rm c}-\theta_{\rm c})} = \frac{L_{\rm int}}{\delta^* G(\theta_{\rm c})} \quad (1)$$

where L^* is the normalized interaction length, $L_{\rm int}$ the interaction length, and δ^* the displacement of the boundary layer upstream of the separation position. The angles, $\theta_{\rm c}$ and $\beta_{\rm c}$, represent the flow deflection and incident shock wave angles, respectively. G is a function that reflects mass conservation [9]. L^* is then correlated with the pressure ratio across the inviscid reflected shock system, $p_{\rm post} / p_\infty$.

Subsequent studies [10–13] revised this scaling law to account for wall cooling, proposing the following semi-empirical formula:

$$L^* \propto \left[\frac{2k}{\gamma M_\infty^2}\left(\frac{C_{\rm f-ad}}{C_{\rm f-is}}\right)^{\alpha}\left(\frac{p_{\rm post}}{p_\infty}-1\right)\right]^{n} \quad (2)$$

where $C_{\rm f}$ is the skin friction coefficient; k is a constant depending on

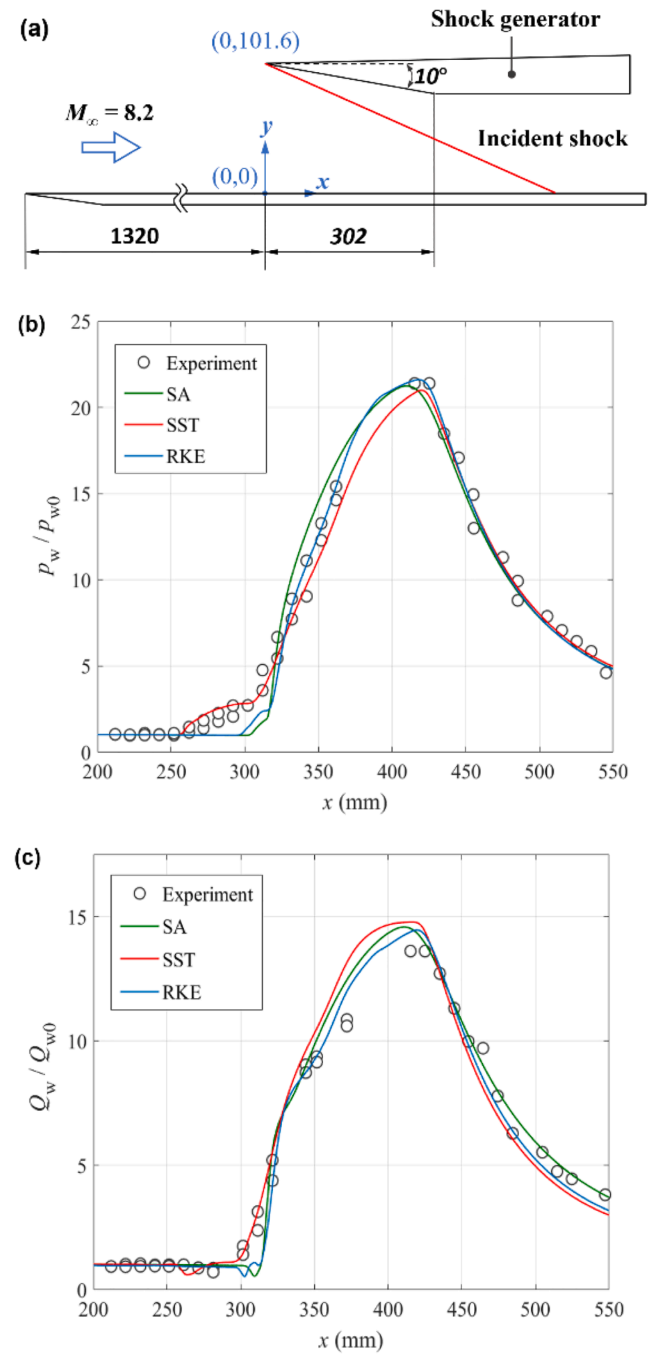

Fig. 3. Non-reacting flow validation: (a) physical model; (b) wall pressure distribution (c) wall heat flux.

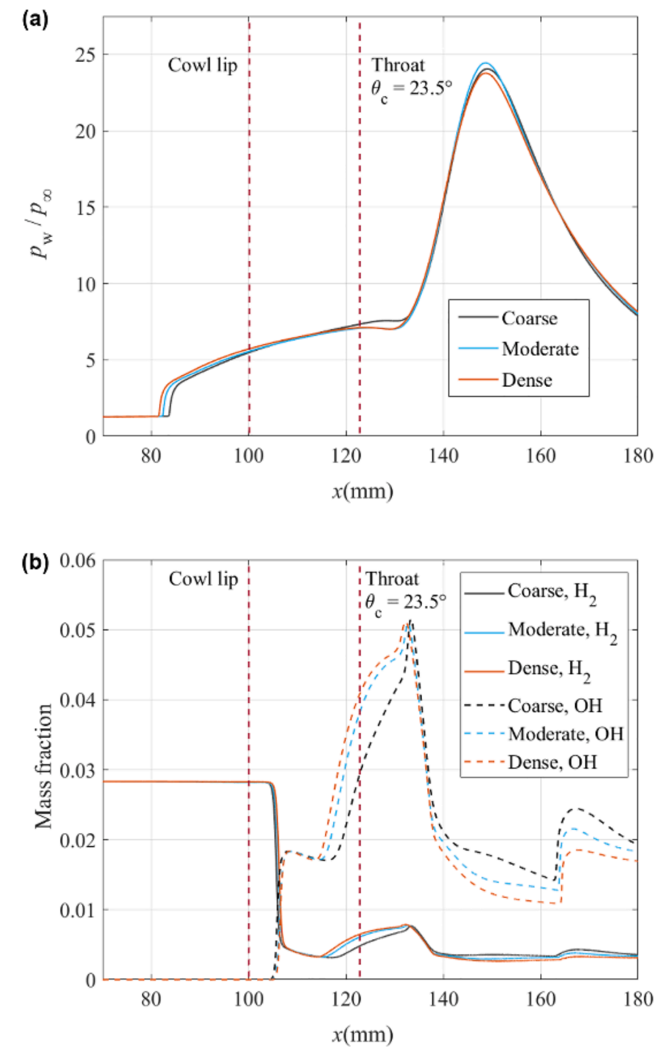

Fig. 4. Grid convergence: (a) wall pressure; (b) mass fractions of key species along the line y = 7.5mm.

Reynolds number; γ is the specific heat ratio; M_∞ is the freestream Mach number; and α and n are constants depending on the gas composition and Reynolds number.

Unlike non-reacting flow, the scaling law for reacting flow must incorporate the effects of combustion heat release, which is the focus of this work. The object is to develop a scaling law applicable to both non-reacting and reacting flows. Separation flow regimes under different static pressures and wall temperatures are simulated using two-dimensional simulations considering detailed chemistry. Theoretical analysis is conducted to formulate the scaling law.

2. Model and numerical methods

The computational model consists of a wedge and a lower flat plate, as illustrated in Fig. 1. A stoichiometric hydrogen/air mixture flows from the left inlet at Mach 7.0. The wedge length Lc ranges from 25 to 45 mm, and the wedge angle θ_c is also adjustable. The height of the wedge lip, h_c, is fixed at 30 mm. To reflect practical ODE conditions where the inlet compresses the air, the inflow static temperature is fixed at 500 K, while the static pressure ranges from 50 to 150 kPa.

The two-dimensional Reynolds-averaged Navier-Stokes equations for viscous, compressible, reactive flow are solved using the finite volume method. Convective fluxes are computed with a second-order total variation diminishing (TVD) scheme coupled with the Harten–Lax–van Leer–Contact (HLLC) Riemann solver. Time integration employs an implicit dual time-stepping method for unsteady simulations, with 40 inner iterations per physical time step of 0.5 μs to reduce the residuals to 10^{-5}. An overset grid method is used, consisting of a background grid and a refined region around the cowl. The first cell height near the wall is within 0.2 μm to ensure that $y^+ < 1$ for the plate wall. To adequately resolve the ODW, the maximum cell size near the contraction duct is smaller than 25 μm. The total grid number is around 3.4 million with grid convergence verified. Detailed hydrogen chemistry [14] is employed. No-slip conditions are applied on the plate wall, with fixed temperatures ranging from 500 to 2000 K. Note that conjugate heat

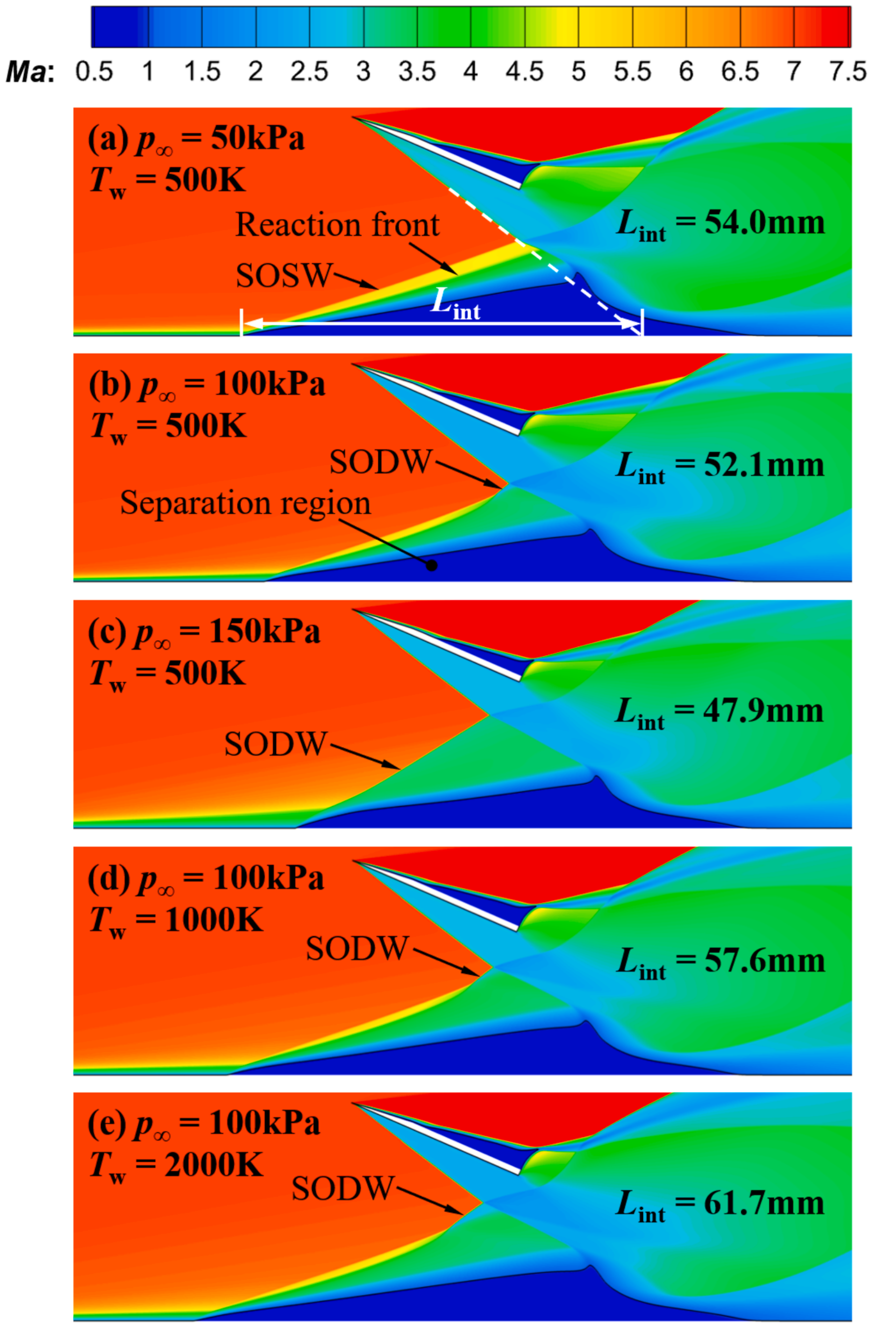

Fig. 5. Separation regimes for varying static pressures and wall temperatures with fixed wedge length of $L_c = 25$mm and wedge angle of $\theta_c = 23.5^\circ$. The black lines denote sonic lines.

transfer in the wall is not considered here. In practical engines, there is cooling within the cool and thereby the conjugate heat transfer is important. Turbulence is modeled using the k-ω SST model with a wall-resolved approach.

Numerical validation is performed against experimental data on supersonic shock-induced combustion [15]. A spherical projectile (15 mm diameter) is launched into stoichiometric hydrogen/air (H_2:O_2:N_2 = 2:1:3.76 molar ratio) or hydrogen/oxygen (H_2:O_2 = 2:1) mixtures at various velocities. For hydrogen/air, the static pressure p_∞, static temperature T_∞, and Mach number Ma are 46.6 kPa, 287 K, and 6.46, respectively. For hydrogen/oxygen, these values are 24.8 kPa, 299 K and 5.08. In Fig. 2(a), the simulated bow shock and reaction front agree with the experimental schlieren images (magenta and green dash lines).

In Fig. 2(b), the green dashed line indicates the overdriven ODW observed experimentally. The simulated standoff distance and wave angle closely match the experimental results, confirming the solver's accuracy in capturing shock-induced combustion and detonation in supersonic hydrogen/oxygen/nitrogen mixtures.

For incident-shock-induced separation, simulation results are compared with experimental data at $Ma = 8.2$ reported by Kussoy and Horstman [16]. In the experiment, a 10° wedge is mounted above the flat plate (see Fig. 3a), with a plate length of 1320 mm upstream of the wedge leading edge. The wedge leading and trailing edges are located at (0, 101.6) mm and (302, 48) mm, respectively. The freestream static pressure and temperature are 430 Pa and 81 K, respectively. The isothermal wall is maintained at 300 K, matching the water-cooled plate in the experiment.

Three turbulence models are evaluated. The pressure distributions in

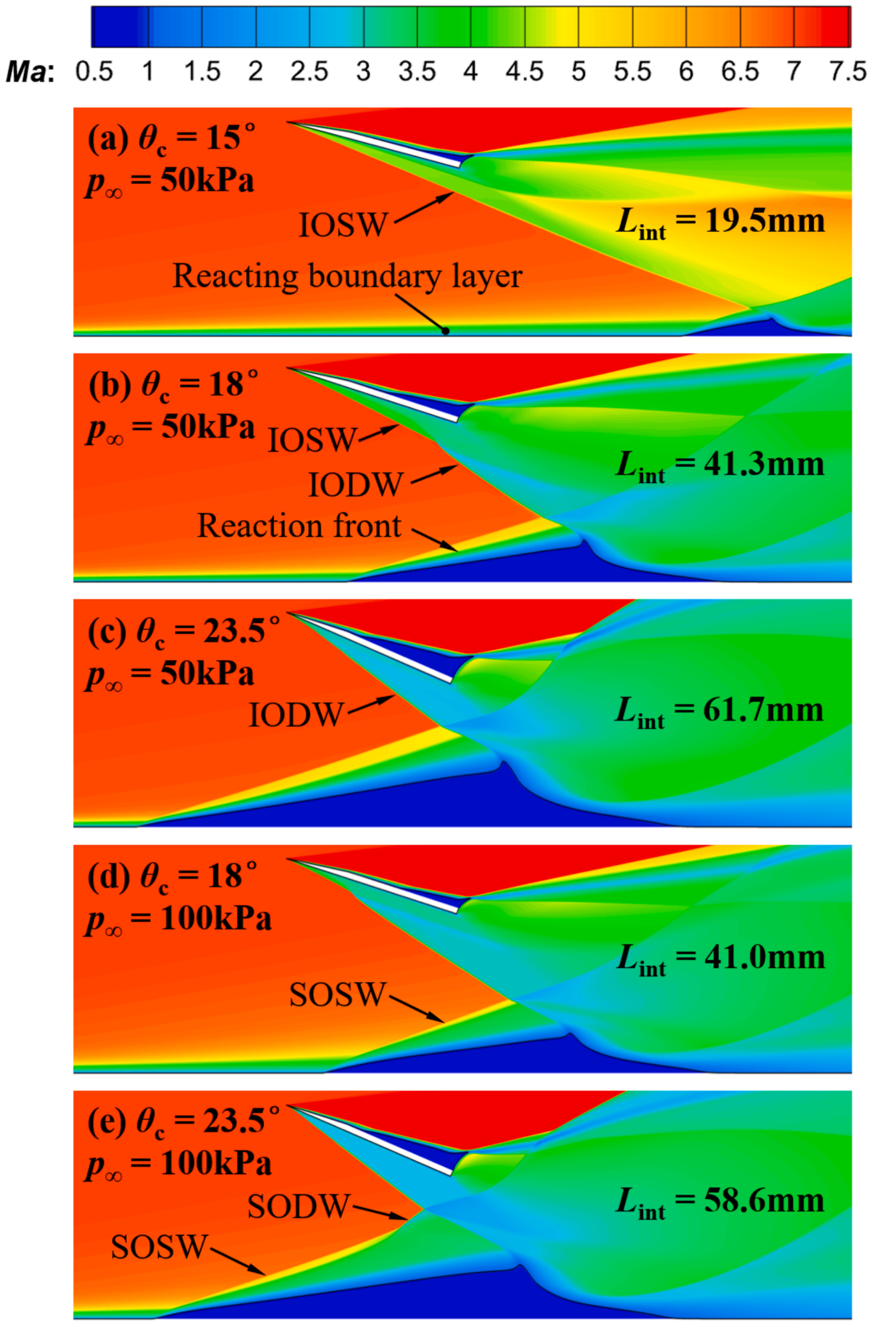

Fig. 6. Separation regimes for varying wedge angles and static pressures with fixed wedge length of L_c = 25mm and wall temperature of T_w = 1200K.

Fig. 3(b) show that the first pressure rise indicates the separation point. The Spalart–Allmaras (S–A) and Realizable k-ε models predict separation further downstream, underestimating the separation scale, whereas the k-ω SST model yields a separation scale consistent with experimental data. In Fig. 3(c), the SST model captures the heat flux drop near the separation point and provides a rising edge closer to the experimental measurements. Therefore, the SST model is adopted in this study.

Grid independence is assessed using three grids with different cell densities. The region containing detonation or shock waves (x = 70 – 190 mm, y = 0 – 40 mm) is refined. The total cell numbers are 1.75, 3.4, and 5.1 million, corresponding to the maximum cell sizes of 60, 35, and 20 μm in the refined region, respectively. The wedge angle is 23.5°; static pressure is 100 kPa; and wall temperature is 1000 K. The wall pressure distributions shown in Fig. 4(a) converge as grid resolution increases. The coarse grid shows a slightly higher pressure plateau within x = 125 – 132 mm. In Fig. 4(b), the mass fractions of H_2 (fuel) and OH (intermediate radical) along the line y = 7.5 mm (which goes through the separation region) indicate that the coarse grid underestimates OH formation, while the medium and fine grids yield consistent results. Therefore, grid independence is achieved with a maximum cell size below 35 μm, and the medium grid is adopted for subsequent simulations.

3. Results and discussion

3.1. ODWBLI and separation regimes

We first examine ODWBLI and separation regimes for various static pressures and wall temperatures, as shown in Fig. 5. In Fig. 5(a), the interaction length of the separation region, L_{int}, is defined as the distance

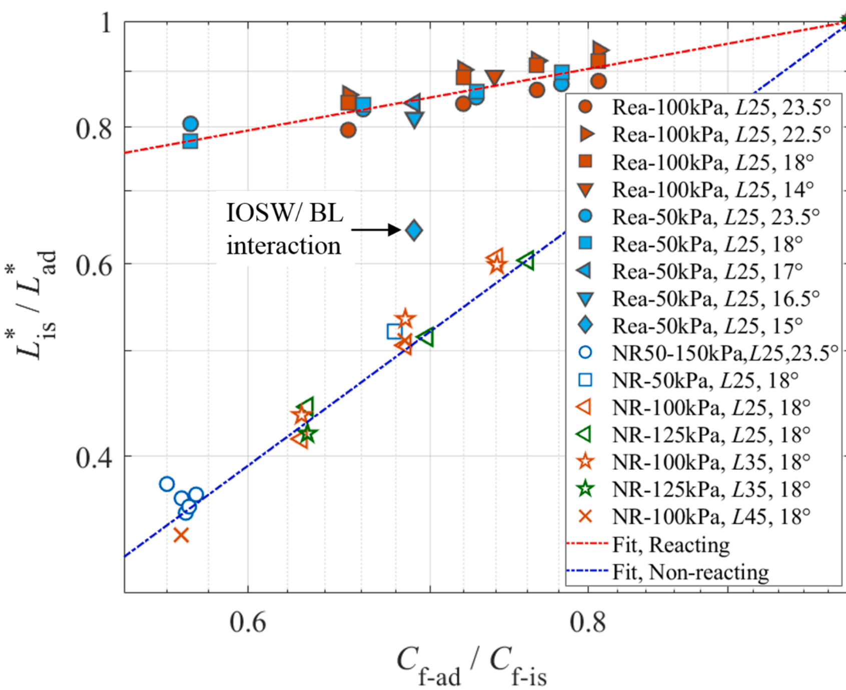

Fig. 7. Variation of dimensionless interaction length with skin friction for reacting and non-reacting flows.

between the separation leading edge and the inviscid impingement position. It is seen that L_{int} decreases with increasing static pressure p_∞. At higher p_∞, the separation oblique shock wave (SOSW) transitions to a separation oblique detonation wave (SODW) due to shorter ignition delay behind the SOSW. Moreover, L_{int} is shown to increase with wall temperature T_w, consistent with boundary-layer characteristics.

Separation regimes for different wedge angles are also investigated (Fig. 6). In Fig. 6(a), for $\theta_c = 15°$, the post-shock temperature behind the incident oblique shock wave (IOSW) is insufficient to initiate detonation at low pressure, resulting in a small-scale separation region characteristic of reacting oblique-shock-wave/boundary-layer interaction (OSWBLI).

For higher pressures or larger wedge angles (Figs. 6b–6e), ODWBLI dominates. As θ_c increases from 18° to 23.5°, L_{int} increases by 49.4% and 42.9% at 50 kPa and 100 kPa, respectively, indicating that separation scale becomes less sensitive to incident wave strength at higher static pressures. This trend cannot be explained by classical theories. According to Eqs. (1) and (2), the effect of θ_c on L_{int} should be more pronounced for lager displacement boundary-layer thickness δ^*. However, δ^* at 100kPa is 1.35 times that at 50kPa due to the near-wall combustion. Therefore, static pressure or Reynolds number influences separation scale through additional mechanisms, including wall heat transfer and heat release.

3.2. Influence of wall temperature and skin friction

We first interpret the effect of wall temperature. From Eq. (2), the relationship between skin friction coefficient C_f and normalized interaction length L^* for adiabatic (with subscript "ad") and isothermal (with subscript "is") walls is:

$$\frac{L^*_{is}}{L^*_{ad}} = \left(\frac{C_{f-ad}}{C_{f-is}}\right)^{\alpha n} \tag{3}$$

This relationship is evaluated for both non-reacting and reacting flows in Fig. 7, using friction coefficients from undisturbed boundary layers. In non-reacting flow, wall heat transfer effects are captured solely by the surface friction coefficient. However, this is not the case in reacting flow. The power exponent αn is 0.45 for reacting flow and 1.83 for non-reacting flow, indicating reduced sensitivity of interaction length to surface friction in reacting flow. Reacting IOSW cases, with weaker wave strength than IODW, exhibit an intermediate slope. This behavior arises because combustion heat release within the boundary layer partially compensates for wall cooling. Hence, Eq. (2) cannot be directly applied to reacting flow.

For subsequent analysis, estimation equations for the skin-friction coefficient on cooled walls are provided. Eukert's reference temperature method [17] is used:

$$T^* = 0.28T_e + 0.5T_w + 0.22T_r \tag{4}$$

$$T_r / T_e = 1 + \frac{1}{2} r(\gamma - 1)M_e^2 \tag{5}$$

where T_e is the static temperature at the boundary- layer edge, and T_r is the recovery temperature (adiabatic wall temperature). Although the recovery factor may be approximated as $r \approx Pr^{1/3}$ for turbulent boundary layer [18], combustion within the boundary layer may increase r. For simplicity, $r = 0.8$ and 0.9 are adopted for non-reacting and reacting flow, respectively.

According to Refs. [19–20], the skin-friction coefficient in compressible turbulent flow is $C_f = 0.0296Re^{-0.2}(T^*/T_e)^{-0.67}$. Therefore, the ratio of adiabatic/isothermal skin friction coefficients is:

$$C_{f-ad} / C_{f-is} = \left(T^*_{ad}/T^*\right)^{-0.67} \tag{6}$$

The exponent is related to the gas viscosity coefficient expressed via power-law formulations. The value remains similar to that of pure air due to the low hydrogen mass fraction in the mixture.

3.3. Heat release effects and coupling mechanisms

The heat release effect is then examined by comparing reacting and non-reacting flow fields in Fig. 8. For the same wedge angle θ_c, the separation scale is significantly enlarged by chemical reactions. As the wall temperature T_w decreases to 500 K, the interaction length L_{int} is reduced by 28.1% in reacting flow, compared to 70.9%7 in non-reacting flow. This stark contrast indicates a strong coupling between wall cooling and combustion heat release near the separation region, where

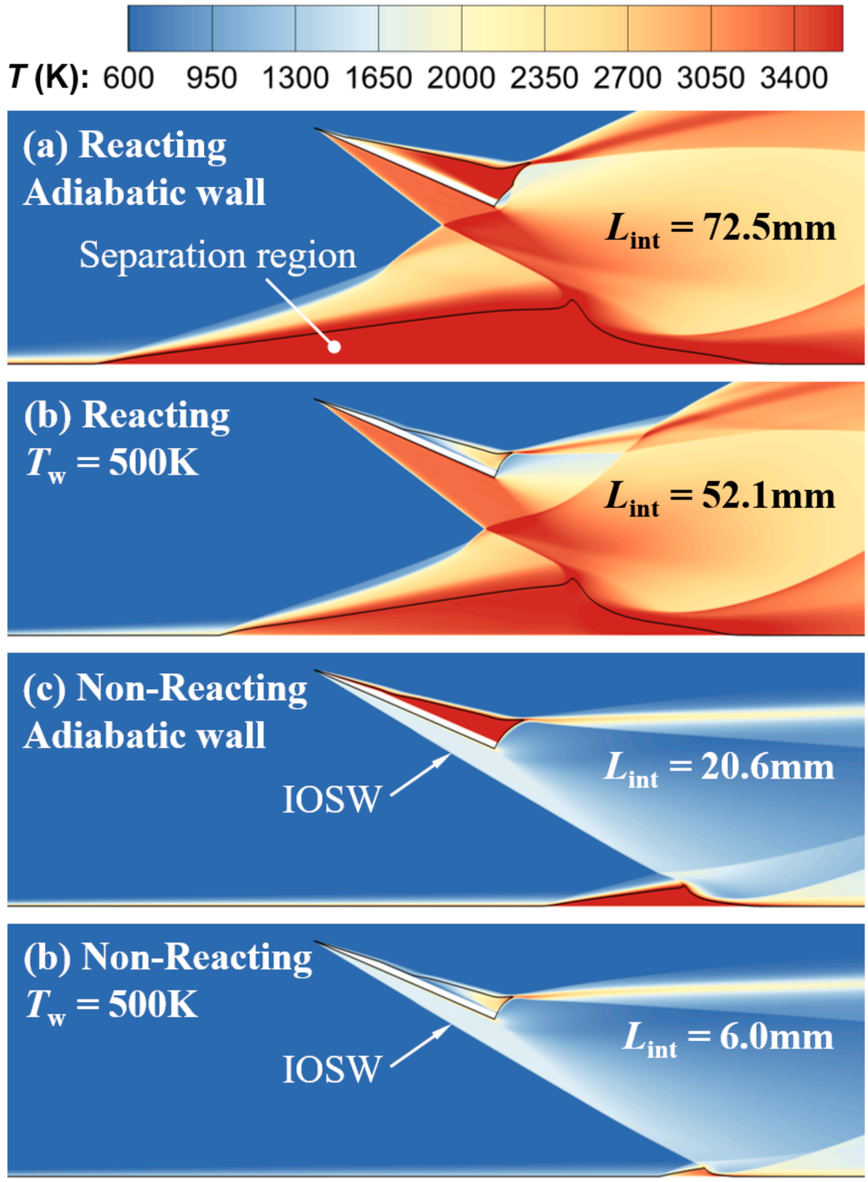

Fig. 8. Reacting andnon-reacting flow fields for different wall temperatures ($p_\infty = 100\text{kPa}$, $L_c = 25\text{mm}$, $\theta_c = 23.5^\circ$).

the latter partially offsets the cooling effect..

To elucidate the underlying mechanisms, Fig. 9 presents a schematic comparison of the separation region structures. In non-reacting flow (top figure), the separation oblique shock wave (SOSW) induces boundary-layer separation without chemical reactions. In reacting flow (bottom figure), the SOSW transitions to a separation oblique detonation wave (SODW) accompanied by a reaction front (RF). The combustion heat release thickens the separation bubble, effectively forming an aerodynamic wedge that modifies the pressure distribution. The height ratio $c = h_D/h_I$ characterizes the reaction front position relative to the wave intersection point, serving as a key parameter for quantifying heat release effects on separation scale.

Consequently, modifications to Eq. (2) must account for heat release, which comprises two independent components: the enhanced pressure difference across the incident wave system, p_{post} / p_∞ - 1, and the heat release behind the SOSW/SODW. In other words, only combustion behind the SOSW or SODW directly enlarges the separation scale relative to non-reacting flow for a given incident pressure difference. Assuming uniform flow behind the SOSW and SODW, the heat release can be expressed as:

$$q_{Rea} = cq_{CVC} + (1-c)q_{SODW} \tag{7}$$

where $c = h_D/h_I$ is the height ratio (see Fig. 9). It is fitted by a function of the static pressure (at very high p_∞, c is limited by the upstream combusting boundary layer):

$$c = \begin{cases} 0.9, p_\infty < 100\text{kPa} \\ 1.7 - 0.008p_\infty, 100\text{kPa} < p_\infty < 150\text{kPa} \\ 0.5, p_\infty > 150\text{kPa} \end{cases} \tag{8}$$

Previous studies approximated combustion on a wedge as constant-volume [21]. The heat release rate for constant-volume combustion on the aerodynamic separation wedge is:

$$q_{CVC} = \sum_{i=1}^{ns} \nu_p U^o_{f,prod} - \sum_{i=1}^{ns} \nu_r U^o_{f,reac} \tag{9}$$

where ns is the species number; and ν_p and ν_f are respectively the stoichiometric coefficients of products and reactants. U^o_f denotes the standard internal energy of formation. Chemical equilibrium and heat release are computed using Cantera [22]. Gas conditions behind the

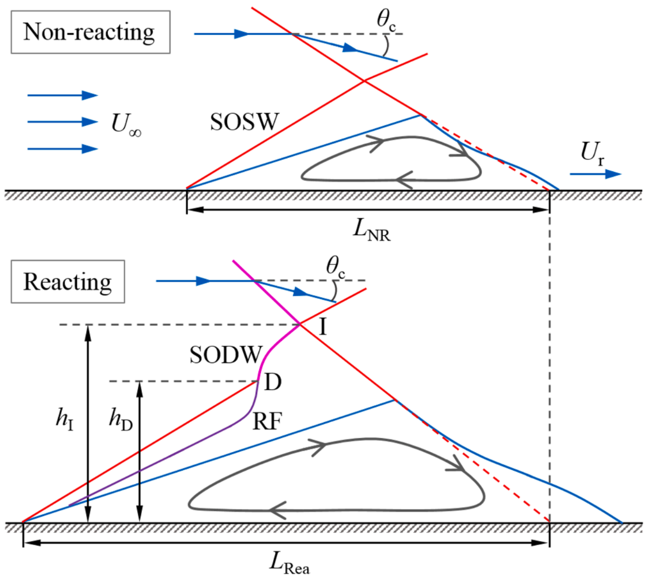

Fig. 9. Schematic flow structure of separation region for non-reacting and reacting flows. SOSW: separation oblique shock wave; SODW: separation oblique detonation wave; RF: Reaction front; D: detonation.

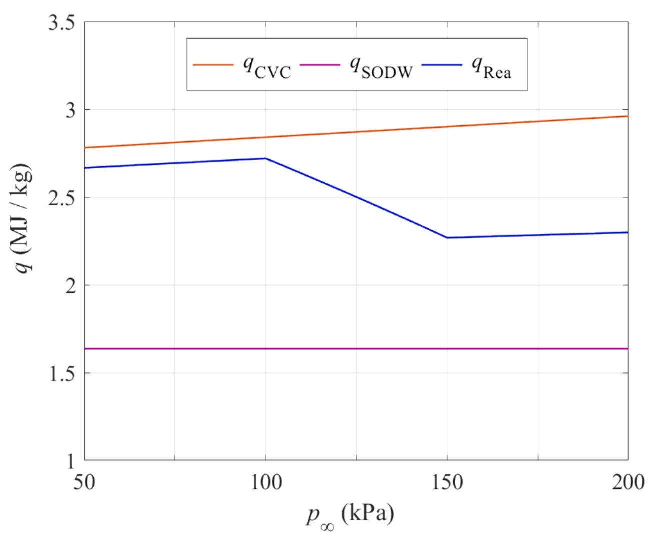

Fig. 10. Characteristic heat release behind the SOSW/SODW as a function of static pressure.

separation shock wave with a wedge angle of 9° are taken as the initial conditions, with static pressure $3.53p_\infty$, static temperature $1.5T_\infty$, and specific heat ratio 1.35.

The heat release of the SODW, q_{SODW}, is calculated by the formula proposed by Teng & Jiang [23], with the wave angle β and the separation angle θ_s obtained from simulations:

$$\frac{\tan\beta}{\tan(\beta-\theta_s)}=\frac{(\gamma+1)Ma^2\sin^2\beta}{\gamma Ma^2\sin^2\beta+1\pm\sqrt{\left(Ma^2\sin^2\beta-1\right)^2-2(\gamma^2-1)Ma^2\sin^2\beta\cdot\frac{\gamma\rho_\infty q_{\mathrm{SODW}}}{p_\infty}}} \tag{10}$$

Figure 10 shows combustion heat release as a function of p_∞. It is observed that q_{SODW} is relatively insensitive to p_∞ and lower than q_{CVC} under the given conditions. Consequently, q_{Rea} decreases with p_∞ at intermediate pressures and remains nearly constant at low and high pressures.

The separation region is sustained by the streamwise momentum and energy balance. In reacting flow, increased dissipation of gas kinetic energy (relative to non-reacting flow) is balanced by combustion heat release. Assuming the velocity near reattachment is proportional to freestream velocity (i.e., $U_r\approx k_1U_\infty$) and independent of heat release, an energy conservation relation is obtained:

$$\eta_0\rho_\infty L_{\mathrm{Rea}}U_\infty q_{\mathrm{Rea}} = \frac{1}{2}\rho_\infty U_\infty\left(U_\infty^2-U_r^2\right)\left(L_{\mathrm{Rea}}-L_{\mathrm{NR}}\right) \tag{11}$$

Here η_0 is a coefficient representing effective combustion heat. L_{Rea} and L_{NR} are the interaction lengths in reacting and non-reacting flow, respectively.

Equation (11) can be rearranged into the formula of L_{nr}^* / L_{Rea}^*. The angle function G in Eq. (1) depends on the wedge angle and heat release. Meanwhile, combustion thickens the upstream boundary layer. As a rough approximation, the ratios of G and δ^* between non-reacting and reacting flows are assumed to be of similar magnitude. For a fixed wedge angle, the interaction length ratio is approximated by:

$$\frac{L_{\mathrm{NR}}}{L_{\mathrm{Rea}}}=\frac{L_{\mathrm{NR}}^*}{L_{\mathrm{Rea}}^*}\frac{\delta_{\mathrm{NR}}^*}{\delta_{\mathrm{Rea}}^*}\frac{G_{\mathrm{Rea}}}{G_{\mathrm{NR}}}\approx\frac{L_{\mathrm{NR}}^*}{L_{\mathrm{Rea}}^*} \tag{12}$$

Substituting Eq. (12) into Eq. (11) yields the following relation between effective combustion heat and dimensionless interaction length:

$$1-\frac{L_{\mathrm{NR}}^*}{L_{\mathrm{Rea}}^*}=\eta\frac{2q_{\mathrm{Rea}}}{U_\infty^2} \tag{13}$$

where the energy conversion efficiency is $\eta=\eta_0$ / (1-k_1^2).

Although η can be determined by modeling detailed flow structures, this study aims to develop an estimation method. According to dimensional analysis [24], the dominant factors are Reynolds number Re, Stanton number St, and skin friction coefficient C_f, respectively corresponding to the effects of boundary-layer thickness, wall heat transfer, and wall friction loss:

$$\eta=f\left(Re,St,C_f\right) =f\left(Re,Pr^{-2/3}C_{f-is},C_{f-ad}/C_{f-is}\right) \tag{14}$$

Here $St = 0.5Pr^{-2/3}C_f$ is known as Chilton-Colburn analogy or modified Reynolds analogy [18,20]. The Prandtl number Pr is fixed at 0.787. Note that for simplicity we intentionally choose fixed Prandtl number, which thereby does not appear explicitly in our scaling law and needs to be explored in future studies. Using Eq. (6) we have $\eta=f$ (Re, T_{ad}*, T*). The simulation data provided in Tables 1 and 2 in the Supplementary Document are processed by this relation, and the results are plotted in Fig. 11.

The relative increase in L^* due to chemical reactions is shown to increase linearly with the effective heat release. After normalization, an empirical formula for η is obtained:

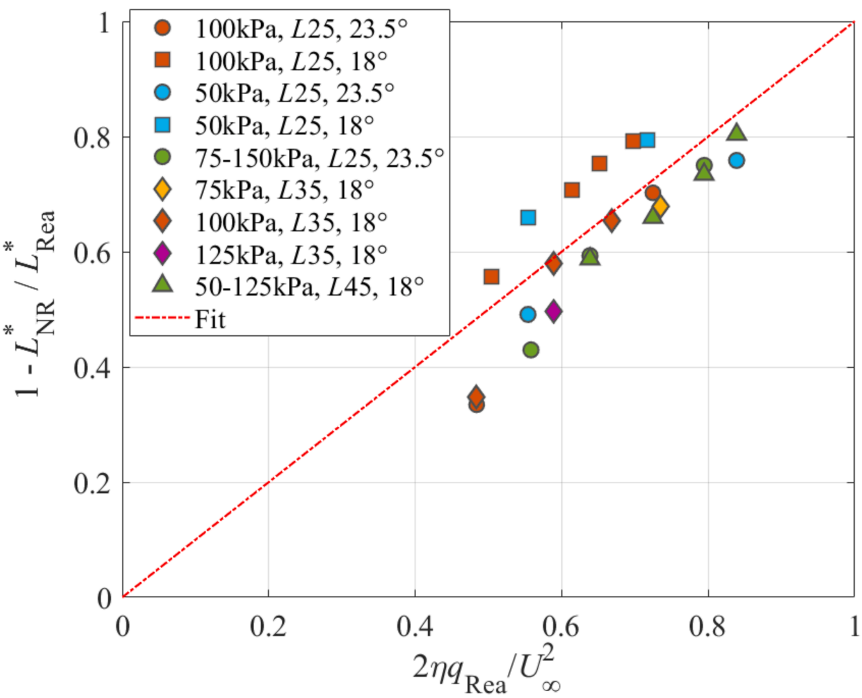

Fig. 11. Relative increase in interaction length versus effective heat release.

$$\eta = 20.5Re^{-0.18}\left(\frac{T_{\rm ad}^*}{T^*}\right)^{0.47} \quad (15)$$

In Fig. 11, the data points collapse into the fitting line with maximum error up to 15%.

3.4. Development of a generalized scaling law

It is noted that the wedge length also affects the separation length scale. As shown in Fig. 12, expansion waves from the wedge trailing edge impinge on the leeward side of the separation region, reducing the streamwise pressure gradient and thus decreasing the separation scale. This effect diminishes as expansion waves move away from the recirculation vortex core, so a longer wedge promotes a larger separation bubble. In non-reacting cases, expansion waves directly weaken the incident shock. As L_c increases from 25 to 35mm, $L_{\rm int}$ increases by 32.4% in reacting flow and 89.4% in non-reacting flow, necessitating distinct treatments of expansion-wave effects for reacting and non-reacting flows.

Our previous study on non-reacting flow [25] showed that the expansion-wave effect is primarily governed by the relative wedge length, yielding the correlation:

$$L_{\rm EW}^* = bL_{\rm NEW}^*\frac{L_c^2}{[(h_c-\delta_c^*)\delta_c^*]} \quad (16)$$

where h_c is the height from the wedge lip to the lower plate. Note that L^* should be corrected when L_c / (h_c - δ^*) < 2.5.

In reacting flow, expansion waves are weakened due to the lower Mach number behind the IODW. A power function incorporating the incident wave type is used for the correction factor. The generalized self-similar formula for reacting/non-reacting interaction length is:

$$L_{\rm EW}^* = b\left(1-\eta\frac{q_{\rm Rea}}{0.5U_\infty^2}\right)^{-1}\left[\left(\frac{T_{\rm ad}^*}{T^*}\right)^{-0.409}\left(\frac{p_{\rm post}}{p_\infty}-1\right)\frac{2}{\gamma M_\infty^2}\right]^3\left[\frac{L_c^2}{(h_c-\delta_c^*)\delta_c^*}\right]^m = bAS^3B \quad (17a)$$

where

$$b = \begin{cases} 1.22, \text{Reacting} \\ 0.195, \text{Non-reacting} \end{cases} \quad (17b)$$

$$m = \begin{cases} 0.5, \text{IODW} \\ 0.75, \text{IOSW(reacting)} \\ 1, \text{Non-reacting} \end{cases} \quad (17c)$$

For non-reacting flow, the correction factor A is 1. For reacting flow, the reference temperature ratio $T_{\rm ad}$* / T* embedded in A partially offsets the same ratio in S, consistent with the reduced sensitivity of reacting L* to $C_{\rm f}$ observed in. Fig. 7.

The simulation data are reprocessed according to Eq. (17), and then the unmodified dimensionless interaction lengths are plotted logarithmically in Fig. 13. The data points collapse into two lines, indicating generalized scaling laws for non-reacting and reacting flows. Due to the lack of experimental data on ODWBLI over flat plate, two non-reacting cases, Kussoy (Ma 8.2, 10°) [16] and Shulein (Ma 5, 14°) [26], are included in Fig. 13. Maximum errors are 17% for reacting flow and 20% for non-reacting flow, which are acceptable for engineering estimates.

Nevertheless, certain limitations should be addressed in future work. First, the height ratio c may be oversimplified, as it is also influenced by wall temperature and separation scale. Second, the physical interpretation of effective heat release requires further investigation, particularly for varying equivalence ratios and Prandtl numbers.

4. Conclusions

This study investigates the oblique-detonation-wave/boundary-layer interaction through numerical simulations of supersonic premixed hydrogen/air flow. The separation scale in reacting flow is quantitatively characterized under various flow conditions and geometric parameters. The dimensionless interaction length correlates with the ratio of adiabatic to isothermal skin friction coefficients, but exhibits significantly reduced sensitivity in reacting flow (power exponent 0.45) compared to non-reacting flow (1.83), as combustion heat release partially offsets wall cooling effects. By introducing the concept of effective heat release within the separation region—expressed as a

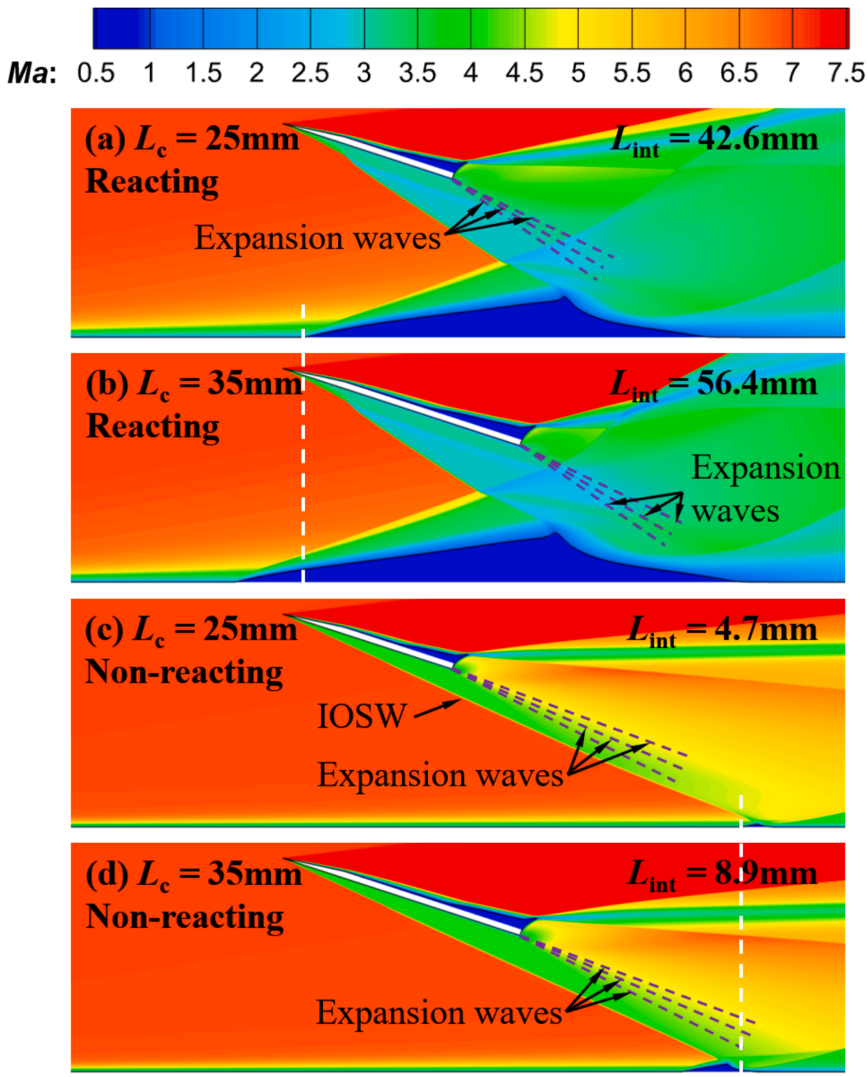

Fig. 12. Reacting and non-reacting flow fields for different wedge lengths with fixed static pressure $p_\infty = 100$ kPa, wall temperatures $T_w = 2000$ K and wedge angle $\theta_c = 18^\circ$.

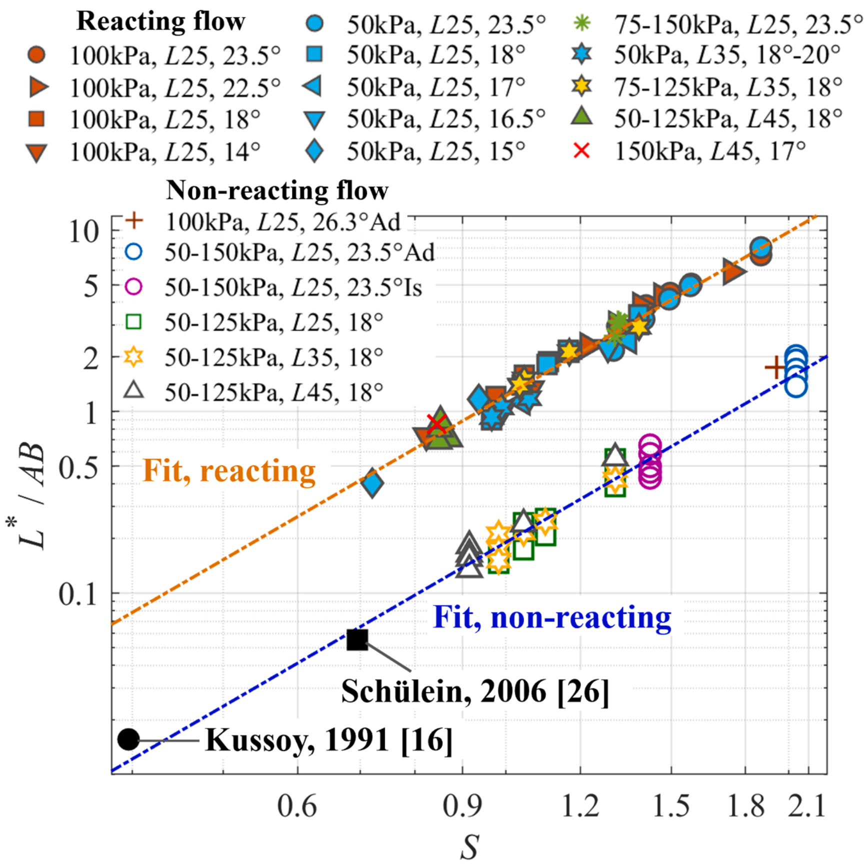

Fig. 13. The scaling law of interaction length for reacting and non-reacting flows.

function of Reynolds number and reference temperature—and incorporating an expansion-wave correction factor, a generalized scaling law is established for both reacting and non-reacting flows. The proposed similarity parameter successfully collapses all simulation data onto two unified curves, yielding maximum errors of 17% for reacting flow and 20% for non-reacting flow. This scaling law provides a quantitative tool for estimating interaction lengths in complex reactive flows.

CRediT authorship contribution statement

Xiaotong Tong: performed research, analyzed data, and drafted and revised the manuscript. **Yufeng Wang**: aided in interpreting the results and revised the manuscript. **Zheng Chen**: designed research, supervision, resources, and revised the manuscript.

Supplementary material associated with this article can be found, in the online version.

Declaration of competing interest

The authors declare that they have no known competing financial interests or personal relationships that could have appeared to influence the work reported in this paper.

Acknowledgements

This work was funded by National Natural Science Foundation of China (Nos. 12402383 and 124B1016).

Supplementary materials

Supplementary material associated with this article can be found, in the online version, at doi:10.1016/j.proci.2026.106144.

References

[1] Z. Jiang, Standing oblique detonation for hypersonic propulsion: a review, Prog. Aerosp. Sci. 143 (2023) 100995.

[2] Z. Zhang, C. Wen, C. Yuan, Y. Liu, G. Han, C. Wang, Z. Jiang, An experimental study of formation of stabilized oblique detonation waves in a combustor, Combust. Flame 237 (2022) 111868.

[3] H. Babinsky, J. Harvey, Shock Wave-Boundary-Layer Interactions, Cambridge University Press, 2011.

[4] K. Wang, H. Teng, P. Yang, H.D. Ng, Numerical investigation of flow structures resulting from the interaction between an oblique detonation wave and an upper expansion corner, J. Fluid Mech. 903 (2020) A28.

[5] Z. Zhang, Y. Liu, C. Wen, Mechanisms of the destabilized Mach reflection of inviscid oblique detonation waves before an expansion corner, J. Fluid Mech. 940 (2022) A29.

[6] H. Yan, X. Han, H. Xiong, C. Shi, Y. You, Curved detonation and its reflections, J. Fluid Mech. 984 (2024) A11.

[7] Z. Zhang, C. Wen, W. Zhang, Y. Liu, Z. Jiang, Formation of stabilized oblique detonation waves in a combustor, Combust. Flame 223 (2021) 423–436.

[8] J. Sun, P. Yang, Z. Chen, Dynamic interaction patterns of oblique detonation waves with boundary layers in hypersonic reactive flows, Combust. Flame 271 (2025) 113832.

[9] L.J. Souverein, P.G. Bakker, P. Dupont, A scaling analysis for turbulent shock-wave/boundary-layer interactions, J. Fluid Mech. 714 (2013) 505–535.

[10] C.M. Helm, M.P. Martín, Scaling of hypersonic shock/turbulent boundary layer interactions, Phys. Rev. Fluids 6 (2021) 074607.

[11] Y. Hong, Z. Li, J. Yang, Scaling of interaction lengths for hypersonic shock wave/turbulent boundary layer interactions, Chinese J. Aeronaut. 34 (2021) 504–509.

[12] F. Zuo, J. Wei, S. Hu, S. Pirozzoli, Effects of wall temperature on hypersonic impinging shock-wave/turbulent-boundary-layer interactions, AIAA J. 60 (2022) 5109–5122.
[13] H. Rathi, K. Sinha, Interaction length analysis of hypersonic shock–boundary-layer interaction including high-enthalpy effects, AIAA J. 62 (2024) 4500–4517.
[14] G.J. Wilson, R.W. Maccormack, Modeling supersonic combustion using a fully-implicit numerical method, AIAA J. 30 (1992) 1008–1015.
[15] H.F. Lehr, Experiments on shock-induced combustion, A. Astronaut. 17 (1972) 589–597.
[16] M.I. Kussoy, K. Horstman, Documentation of two- and three dimensional shock-wave/turbulent-boundary-layer interaction flows at Mach 8.2, NASA Ames Res. Center (1991). NASA-TM-101075.
[17] E. Eckert, Engineering relations for heat transfer and friction in high-velocity laminar and turbulent boundary-layer flow over surfaces with constant pressure and temperature, Trans. Am. Soc. Mech. Eng. 78 (1956) 1273–1283.
[18] H. Schlichting, K. Gersten, Boundary-layer theory, 9th ed., Springer, 2017.
[19] G. Simeonides, Generalized reference-enthalpy formulation and simulation of viscous effects in hypersonic flow, Shock Waves 8 (1998) 161–172.
[20] E.H. Hirschel, Basics of aerothermodynamics, 2nd ed., Springer International Publishing, 2015, pp. 248–258.
[21] H. Teng, H.D. Ng, Z. Jiang, Initiation characteristics of wedge-induced oblique detonation waves in a stoichiometric hydrogen-air mixture, Proc. Combust. Inst. 36 (2017) 2735–2742.
[22] Cantera, https://cantera.org/.
[23] H. Teng, Z. Jiang, On the transition pattern of the oblique detonation structure, J. Fluid Mech. 713 (2012) 659–669.
[24] G.I. Barenblatt, Scaling, Cambridge University Press, 2003.
[25] X. Tong, Q. Zhang, W. Wu, L. Yue, C. He, Z. Chen, Generalized similarity laws for unstart phenomenon of contraction ducts in supersonic flow, AIAA J. 63 (2025) 4682–4700.
[26] E. Schülein, Skin-friction and heat flux measurements in shock/boundary-layer interaction flows, AIAA J. 44 (2006) 1732–1741.